Characterization of an Acetone Detector based on a Suspended WO3-Gate AlGaN/GaN HEMT Integrated with Micro-heater

Sun, Jianwen; Sokolovskij, Robert; Iervolino, Elina; Santagata, Fabio; Liu, Zewen; Sarro, Pasqualina M.; Zhang, Guogi

DOI
10.1109/TED.2019.2936912

Publication date
2019

Document Version
Final published version

Published in
IEEE Transactions on Electron Devices

Characterization of an Acetone Detector Based on a Suspended WO_3-Gate AlGaN/GaN HEMT Integrated With Microheater

Jianwen Sun, Robert Sokolovskij, Elina Iervolino, Fabio Santagata, Zewen Liu, Pasqualina M. Sarro, *Fellow, IEEE*, and Guoqi Zhang, *Fellow, IEEE*

***Abstract*— A suspended AlGaN/GaN high electron mobility transistor (HEMT) sensor with a tungsten trioxide (WO_3) nanofilm modified gate was microfabricated and characterized for ppm-level acetone gas detection. The sensor featured a suspended circular membrane structure and an integrated microheater to select the optimum working temperature. High working temperature (300°C) increased the sensitivity to up to 25.7% and drain current change I_{DS} to 0.31 mA for 1000-ppm acetone in dry air. The transient characteristics of the sensor exhibited stable operation and good repeatability at different temperatures. For 1000-ppm acetone concentration, the measured response and recovery times reduced from 148 and 656 to 48 and 320 s as the temperature increased from 210 °C to 300 °C. The sensitivity to 1000-ppm acetone gas was significantly greater than the sensitivity to ethanol, ammonia, and CO gases, showing low cross-sensitivity. These results demonstrate a promising step toward the realization of an acetone sensor based on the suspended AlGaN/GaN HEMTs.**

***Index Terms*— Acetone sensor, AlGaN/GaN, gas sensor, high electron mobility transistor (HEMT), WO_3.**

Manuscript received July 6, 2019; revised August 18, 2019; accepted August 18, 2019. Date of publication September 2, 2019; date of current version September 20, 2019. This work was supported by the Beijing Delft Institute of Intelligent Science and Technology. The review of this article was arranged by Editor M. M. Hussain. *(Corresponding authors: Pasqualina M. Sarro; Guoqi Zhang.)*

J. Sun is with the Department of Microelectronics, Delft University of Technology, 2628 CD Delft, The Netherlands, and also with the China Research Institute, Delft University of Technology, 100083 Beijing, China (e-mail: sunjw15@163.com).

R. Sokolovskij is with the Department of Microelectronics, Delft University of Technology, 2628 CD Delft, The Netherlands, also with the Department of Electrical and Electronic Engineering, Southern University of Science and Technology, Shenzhen 518055, China, and also with the State Key Laboratory of Solid State Lighting, Changzhou 213161, China (e-mail: r.sokolovskij@tudelft.nl).

E. Iervolino is with USound Shenzhen Office, Shenzhen 518057, China (e-mail: Elina.iervolino@usound.com).

F. Santagata is with Shenzhen 3NOD Acousticlink Company, Ltd., Shenzhen 518030, China (e-mail: fabio@3nod.com.cn).

Z. Liu is with the Institute of Microelectronic, Tsinghua University, Beijing 10084, China (e-mail: liuzw@tsinghua.edu.cn).

P. M. Sarro and G. Zhang are with the Department of Microelectronics, Delft University of Technology, 2628 CD Delft, The Netherlands (e-mail: p.m.sarro@tudelft.nl; g.q.zhang@tudelft.nl).

Color versions of one or more of the figures in this article are available online at http://ieeexplore.ieee.org.

Digital Object Identifier 10.1109/TED.2019.2936912

I. Introduction

ACETONE as a volatile, flammable, and irritant odor organic solvent has been extensively used in industrial applications, particularly in the pharmaceutical industry and for pesticide preparation. In addition, long-term exposure to high concentrations of acetone (more than 1000 ppm) may endanger human health, causing headache, fatigue, coma, and even death [1]. Therefore, the detection of acetone concentration is an urgent and crucial matter, especially in view of public safety and human health.

A variety of analytical techniques, such as gas/liquid chromatography [2], electrochemistry [3], infrared spectroscopy [4], and semiconductor [5], have been proposed for acetone detection. Among these techniques, the sensors based on semiconductors have the attractive features of a fast response, low power consumption, and compact size. Most of the research into the semiconductor sensors have focused on metal oxide semiconductors such as ZnO [5]–[7], SnO_2 [8]–[10], WO_3 [11]–[13], NiO [14], [15], In_2O_3, and Fe_2O_3 [16]–[19]. Tungsten trioxide (WO_3) is an n-type bandgap semiconductor material and has excellent properties for gas detection because it shows a high catalytic behavior both in oxidation and reduction reactions on its surface [20].

The AlGaN/GaN heterojunction structure is an attractive choice for gas detectors because of its robust performance in harsh environments. Many types of GaN-based devices have been studied for gas and chemical detection. Among them are Schottky diodes, metal oxide semiconductor (MOS) diodes, and AlGaN/GaN high electron mobility transistors (HEMTs). Compared with a Schottky diode, the AlGaN/GaN HEMT structure exhibits great current changes to the surface charges created by the reaction to the target gases or chemical substances and lower theoretical detection limits. This is introduced by the higher carrier density two-dimensional electron gas (2-DEG) introduced by piezoelectric and spontaneous polarization at the interface between AlGaN and GaN layers. AlGaN layers with 30% Al concentration contain 5–10 times higher channel sheet densities compared with GaAs or InP HEMTs. By functionalizing the gate area of an HEMT sensor for sensing materials, the AlGaN/GaN sensors

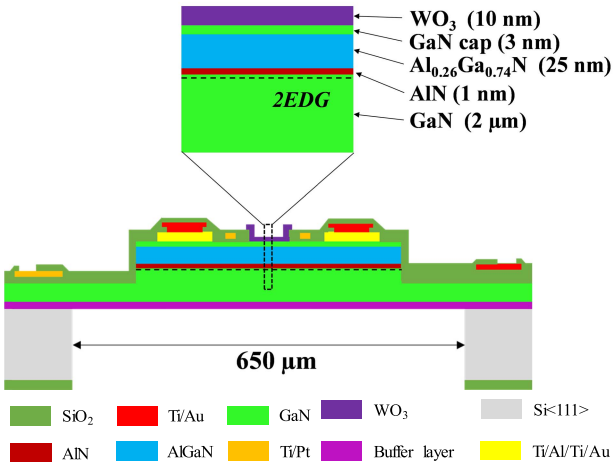

Fig. 1. Schematic cross section of the HEMT sensor structure.

have been demonstrated for H_2 [21], CO [22]–[24], NO [25], [26], NO_2 [26]–[28], NH_3 [25], [29], [30], CH_4 [31], H_2S [32], [33], and C_2H_2 [34]. So far, very few results of acetone detection with AlGaN/GaN devices have been reported [35].

As for most of the chemical sensing, the important parameters such as selectivity, sensitivity, and response/recovery time of the gas sensors can be promoted by increasing the surface temperature. External heating element can be used to achieve the required temperature. However, it is may not be feasible for some applications. Therefore, integrating a heating unit is an attractive alternative to elevate sensor performance [36].

In this article, we demonstrate the successful sensing of acetone vapor using a suspended WO_3-gate AlGaN/GaN HEMT sensor with an integrated microheater. The transient characteristics of the sensor at various surface temperatures and acetone concentrations under room temperature and in dry air ambient are investigated. The sensor shows a current increase and rapid response to different acetone concentrations. Moreover, the selectivity and reproducibility of the sensor are demonstrated.

II. Experiment

A. Fabrication

Fig. 1 presents a schematic of the device cross section. The HEMT sensor is fabricated together with the microheater surrounding the source/gate/drain area on a suspended membrane. The contact pads are on a thick silicon frame.

The epitaxial structure was grown on a 2-in silicon <111> wafer using metal-organic chemical vapor deposition. Starting from the substrate, the structure consisted of a 2-μm-thick undoped GaN buffer layer, followed by a 1-nm-thick AlN interlayer, an undoped 25-nm-thick $Al_{0.26}Ga_{0.74}N$ barrier layer, and a 3-nm-thick GaN epitaxial cap layer. The fabrication process flow started with a mesa etching using a chlorine/boron chloride (Cl_2/BCl_3) plasma to define the sensor geometry. Then, Ti/Al/Ti/Au (20/110/40/50 nm) metal contacts were e-beam evaporated and patterned by the lift-off technology. A rapid thermal annealing at 870°C for 45 s under N_2 ambient was performed to obtain an ohmic contact. Then, a Ti/Pt (30/200 nm) metal layer as the microheater layer was

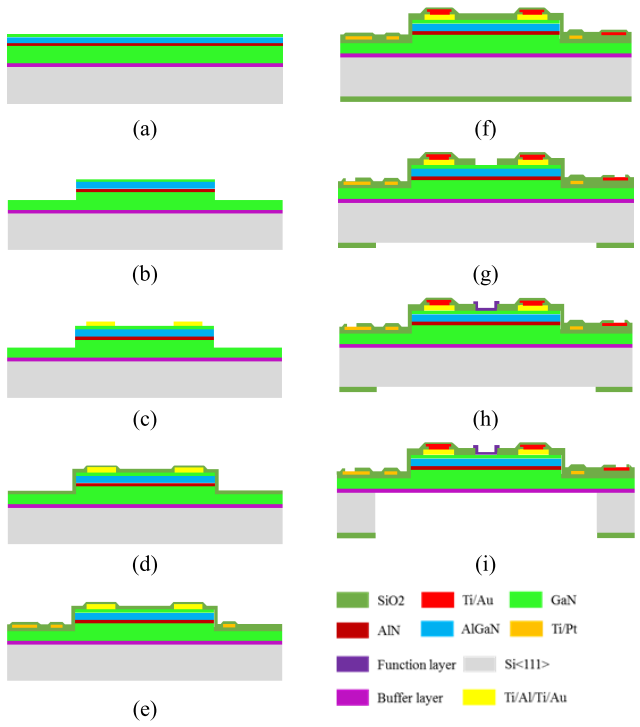

Fig. 2. Main steps for the fabrication of the suspended AlGaN/GaN HEMT sensor integrated with microheater. (a) Starting wafer with epitaxial layers. (b) Mesa etching to define the sensor area. (c) Ohmic contact deposition and annealing. (d) PECVD SiO_2. (e) Microheater deposition and passivation. (f) Metal deposition and top/bottom passivation. (g) Opening contact pads at the frontside and etching window at the backside. (h) Functional material deposition. (i) Substrate etching from the backside to form the suspended structure.

evaporated and patterned by the lift-off process, followed by a SiO_2 layer as the isolation layer. Then the metal interconnect was formed using an evaporated Ti/Au (20/300 nm) layer stack. A 5-μm-thick SiO_2 layer as hard mask during the DRIE process to etch the silicon substrate and the topside SiO_2 layer as the passivation layer were deposited. The WO_3 (10 nm) layer was then deposited on the gate area of 80 μm × 40 μm by physical vapor deposition (PVD). The silicon substrate is etched away below the active area in the final step, thus forming the membrane and the suspended sensor structure. The main steps of the fabrication processes are shown in Fig. 2. More details can be found in our early work [32].

The microheater has a rectangular geometry around a central area of 230 μm × 290 μm, as shown in Fig.3(a). Fig.3(b) shows the SEM images of the AlGaN/GaN HEMTs and the atomic force microscope (AFM) image and profile of the 10-nm WO_3 layer.

B. Characterization

After dicing, the chips were wire-bonded to a ceramic quad flat no-lead (CQFN) package with a size of 4 mm × 4 mm [Fig. 2(c)]. This sensor package is designed to eliminate the effect of gas flow by a perforated lid. The 8-pin QFN testing socket is placed in a gas chamber and electrically connected to a Keithley 2400 source meter. The target gas was injected into the test chamber by a microinjector. The target liquid, for example, acetone and ethanol, injected into the chamber was

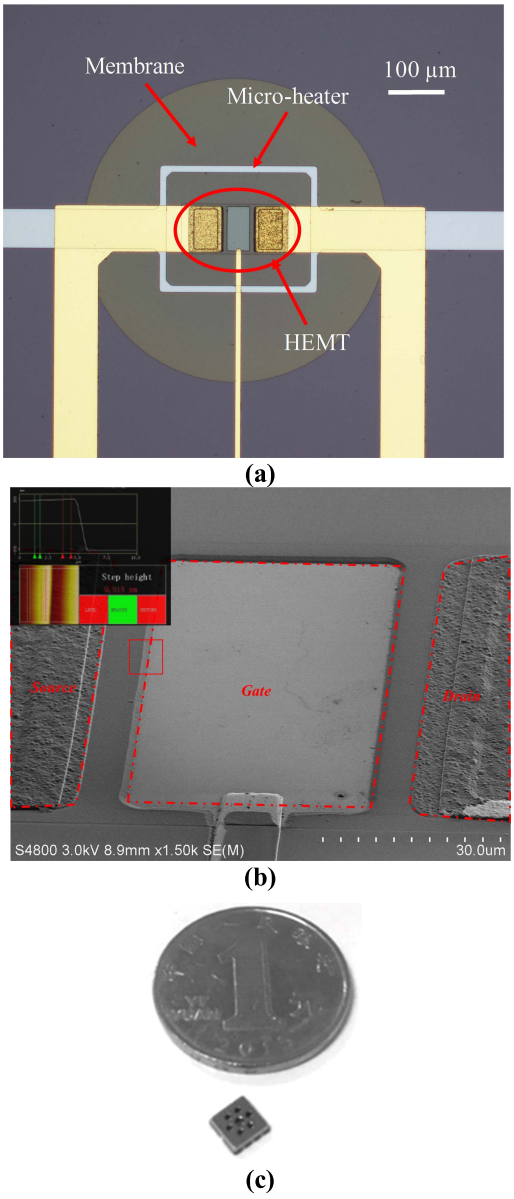

Fig. 3. (a) Top optical micrograph of the fabricated sensor. (b) SEM image of the HEMT sensor. The inset is the AFM image and step height of 10-nm WO_3 layer taken in the red solid line area indicated. (c) Optical photograph of CQFN packaged sensor beside a coin.

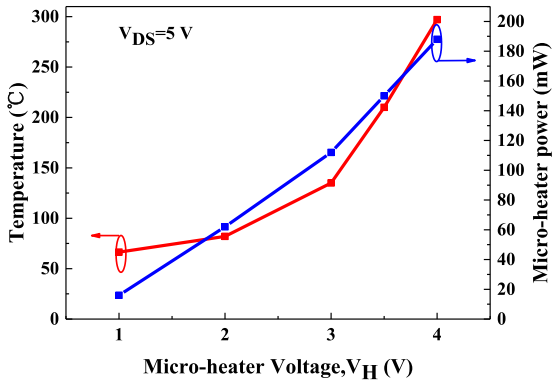

Fig. 4. Measured heating power consumption of the microheater and temperature versus microheater voltage at $V_{DS} = 5$ V.

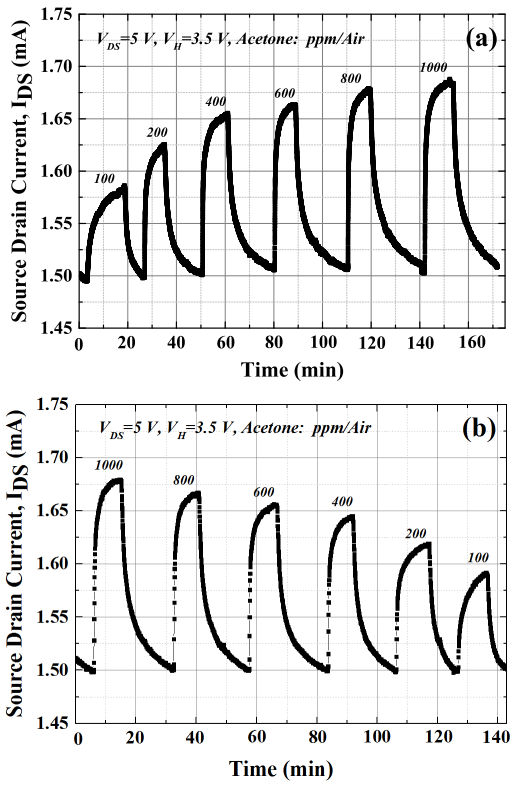

Fig. 5. Transient response characteristics upon injection and purge of acetone in dry air ambient. During all measurements $V_{DS} = 5$ V and $V_H = 3.5$ V. (a) With concentration increasing. (b) With concentration decreasing.

evaporated. After the drain current reached a new saturation, the test chamber was opened and the gas was removed by a micro air pump. The gas sensitivity was designated as $S(\%) = (\Delta I_{DS})/(I_{DS,air}) \times 100\%$, where $\Delta I_{DS} = I_{DS,acetone} - I_{DS,air}$ is the drain current change between acetone and air ambient. The response time (t_{Res}) and recovery time (t_{Rec}) were defined as the time required for the drain current to change/return from 10% to 90% of its saturated response value to acetone gas.

III. Results and Discussion

To extract the membrane temperature, a calibration of the membrane temperatures is necessary. The surface temperature can be measured by infrared radiation (IR) thermal camera (Bruker) or extracted by the resistance change in the microheater at ambient temperature with the four-wire testing method [37]. Fig. 4 shows the measured maximum temperatures and microheating power consumption of the suspended AlGaN/GaN membrane at various applied microheater voltages (V_H). For $V_H = 3.5$ V and $V_H = 4$ V, the maximum gate surface temperatures are calculated to be about 210°C and 300°C. The power consumption of the sensor is about 200 mW when the operating temperature is about 300 °C. To further improve the heating efficiency, a larger size membrane and cyclic heating [36] can be used.

A. Response to acetone in Air

Fig. 5 shows the transient performance of the WO_3 HEMT sensors at the applied microheater voltage ($V_H = 3.5$ V) in

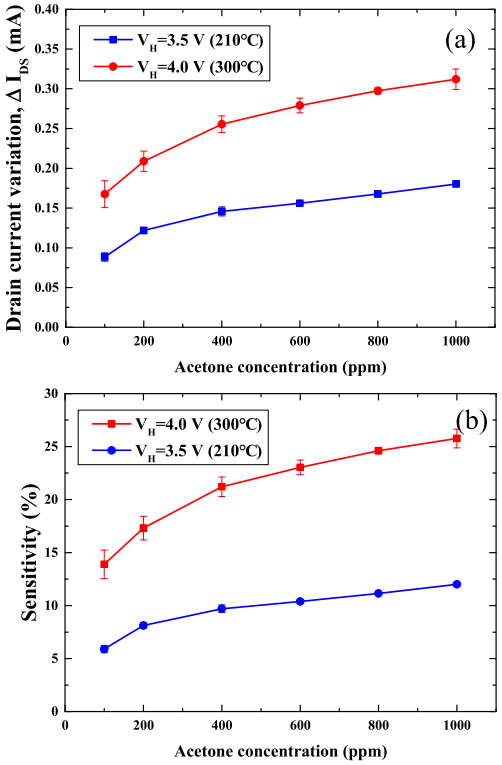

Fig. 6. (a) Drain current variation and (b) sensitivity as a function of acetone concentration for $V_{DS} = 5$ V, $V_H = 3.5$ V (210 °C), and $V_H = 4$ V (300 °C).

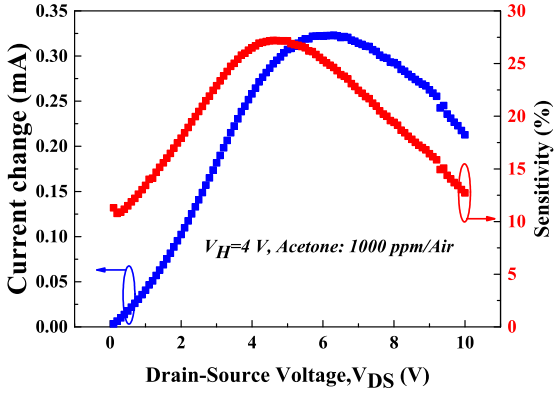

Fig. 7. Current change and sensitivity to 1000-ppm acetone at different drain–source voltage (V_{DS}).

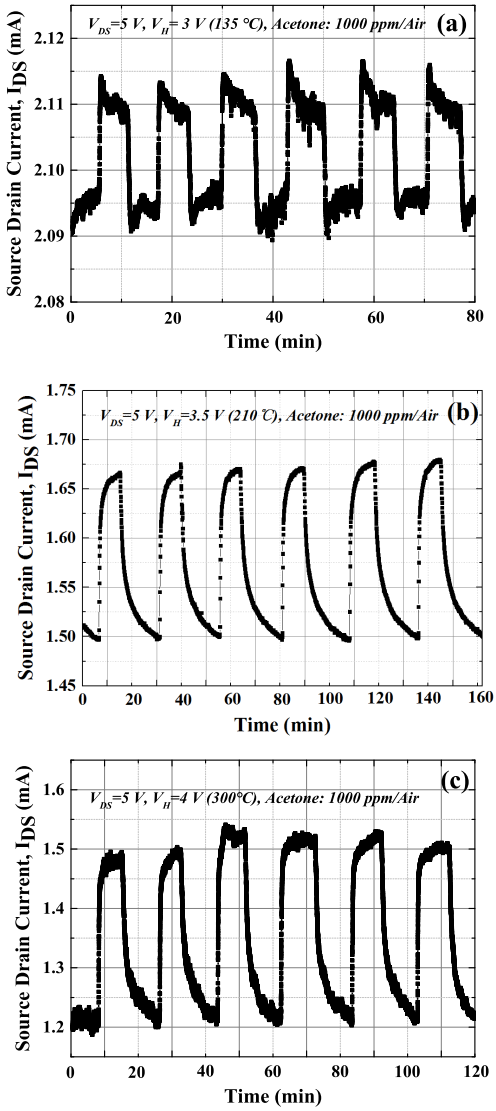

Fig. 8. Six repetitive cycles of sensor exposure to 1000-ppm acetone at (a) $V_H = 3$ V (135 °C),(b) $V_H = 3.5$ V (210 °C),and (c) $V_H = 4$ V (300 °C).

the gas concentration range from 100 to 1000 ppm. Upon exposure to acetone, the source–drain current increases from the baseline value in dry air. The sensor shows stable operation and good repeatability, both for increasing [Fig.5(a)] and decreasing [Fig.5(b)] gas concentration.

An important sensor parameter is the magnitude of sensing signal variation ΔI_{DS}. Previously reported gas sensors based on AlGaN/GaN Schottky diodes show very high sensitivities, in the order of 1000% at ppm-level gas concentrations. However, the current change was in nA–μA range, due to the low baseline signal values. Low ΔI_{DS} will result in higher noise susceptibility of the sensor and higher limit of detection. Fig. 6 shows the drain–source current change and sensitivity as a function of acetone concentration for $V_{DS} = 5$ V at $V_H = 3.5$ V (210°C) and $V_H = 4V$ (300°C). It is obvious that the response increased at a higher temperature. In this work, for 1000-ppm acetone concentration, the measured ΔI_{DS} and sensitivity showed an almost twofold increase, from 0.18 mA (12%) at $V_H = 3.5$ V to 0.31 mA (25.7%) at $V_H = 4$ V, while at 100 ppm $\Delta I_{DS} = 0.16$ mA, which is larger than the reported value of $\Delta I \sim 12$ μA at 100-ppm acetone for a Schottky-type sensor [35], [38]. Figs. 5 and 6 show that lower concentration of acetone could be expected due to the large drain current change.

The drain current change and sensitivity to 1000-ppm acetone at different drain–source voltage are shown in Fig. 7. The current variation and sensitivity increase when V_{DS} increases from 0 to 5 V. However, the current change and sensitivity decrease with an increase in V_{DS}, due to the sensor working in the saturation range. The optimized V_{DS} of this sensor is around 5 V.

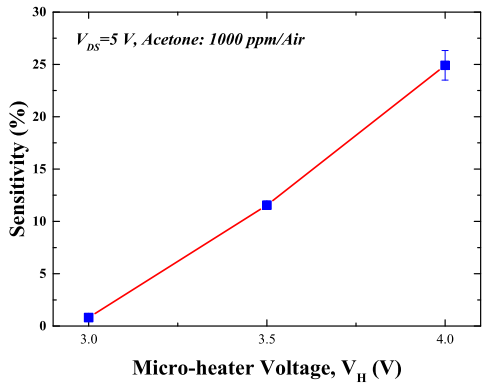

Fig. 9. Sensitivity to 1000-ppm acetone at different microheater voltages (temperature).

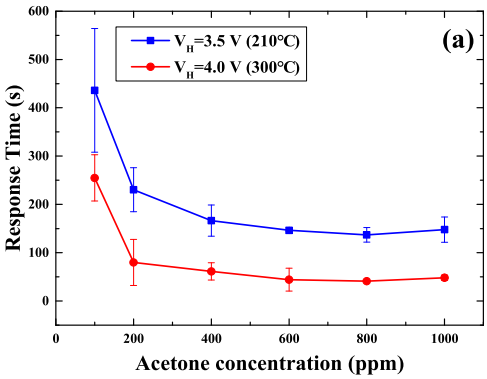

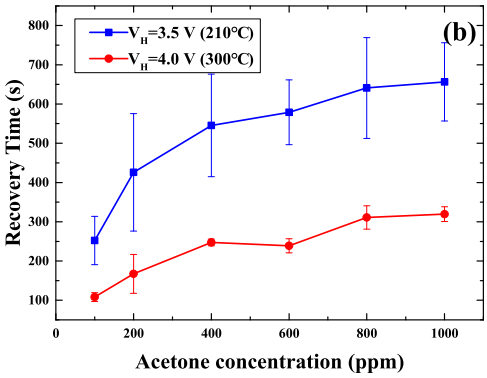

Fig. 10. (a) Response time and (b) recovery time versus acetone concentration at $V_H = 3.5$ V (210 °C) and $V_H = 4$ V (300 °C).

The repeatability of the sensor measured at $V_H = 3$ V (135 °C), $V_H = 3.5$ V (210 °C), and $V_H = 4$ V (300 °C) is shown in Fig. 8. The drain current response to acetone gas when the acetone concentration is swept back and forth from 0 to 1000 ppm is reported.

The effect of the working temperature, known to have a great influence on the sensitivity of the gas sensor, was studied as well. Six repetitive cycles of sensor exposure to 1000-ppm acetone at various working temperatures regulated by the integrated microheater voltage are shown in Fig. 8. The sensitivity as a function of the microheater voltage is plotted in Fig. 9. The sensitivity of the sensor exposed to 1000-ppm acetone at $V_H = 3$ V (135 °C), $V_H = 3.5$ V (210 °C), and $V_H = 4$ V (300 °C) is 0.8%, 12%, and 25.7%, respectively.

TABLE I
RESPONSE TIME AND RECOVERY TIME VERSUS ACETONE CONCENTRATION AND TEMPERATURES

Acetone conc. (ppm)	t_{Res} (s)		t_{Rec} (s)	
	210 ℃	300 ℃	210 ℃	300 ℃
100	*436*	*255*	*252*	*108*
200	*230*	*80*	*426*	*167*
400	*166*	*61*	*545*	*247*
600	*146*	*44*	*579*	*239*
800	*137*	*41*	*641*	*311*
1000	*148*	*48*	*656*	*320*

t_{Res}= response time; t_{Rec}= recovery time.

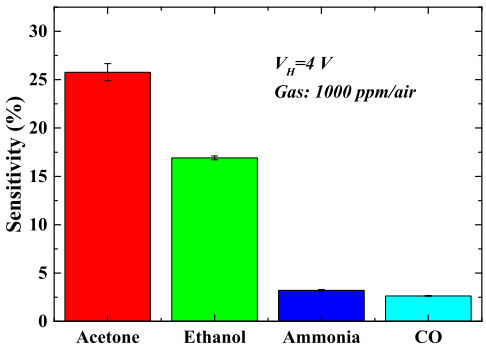

Fig. 11. Gas sensing response to 1000 ppm of acetone, ethanol, ammonia, and CO at $V_H = 4$ V.

Fig. 10 characterizes t_{Res} and t_{Rec} as a function of acetone concentration at the applied microheater voltages. The transient response times decreased with increasing gas concentration for $V_H = 3.5$ V (210 °C) and $V_H = 4$ V (300 °C), while the recovery times increased with increasing gas concentration. From a concentration of 400 ppm, t_{Res} is stable. The response time and recovery time at different temperatures are shown in Table I. At 1000-ppm acetone concentration, t_{Res} (t_{Rec}) reduced from 148 (656) s at $V_H = 3.5$ V (210 °C) to 48 (320) s at $V_H = 4$ V(300 °C). At the concentration of 100 ppm, t_{Res} (t_{Rec}) also decreased from 436 (255) s to 252 (108) s with increasing temperature. The shorter response (recovery) time is attributed to faster gas adsorption and desorption rate at the gate surface under higher temperature.

Another important characteristic of the sensor is selectivity. Fig. 11 presents the acetone selective performance of the HEMT sensor to other typical interfering gases such as ethanol, ammonia, and CO at $V_H = 4$ V. The sensor sensitivity to 1000-ppm acetone is 25.7% and the sensitivity to ethanol, ammonia, and CO is as low as 16.9%, 3.2%, and 2.6%, respectively. It is evident that the HEMT gas sensor exhibits good selectivity toward acetone. The humidity effect at different temperatures is shown in Fig. 12. The effect of the relative humidity on I_{DS} becomes insignificant with increasing temperature.

B. Sensing Mechanism of WO_3/AlGaN/GaN Sensor

Previously, it was found that the gas molecules containing oxygen, upon adsorption on the surface of the catalytic metals

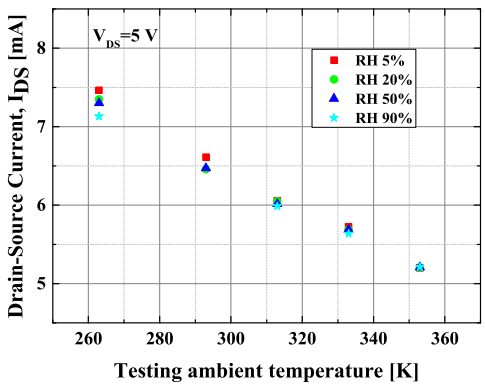

Fig. 12. Relative humidity effect on the I_{DS} of the sensor at $V_{DS} = 5$ V.

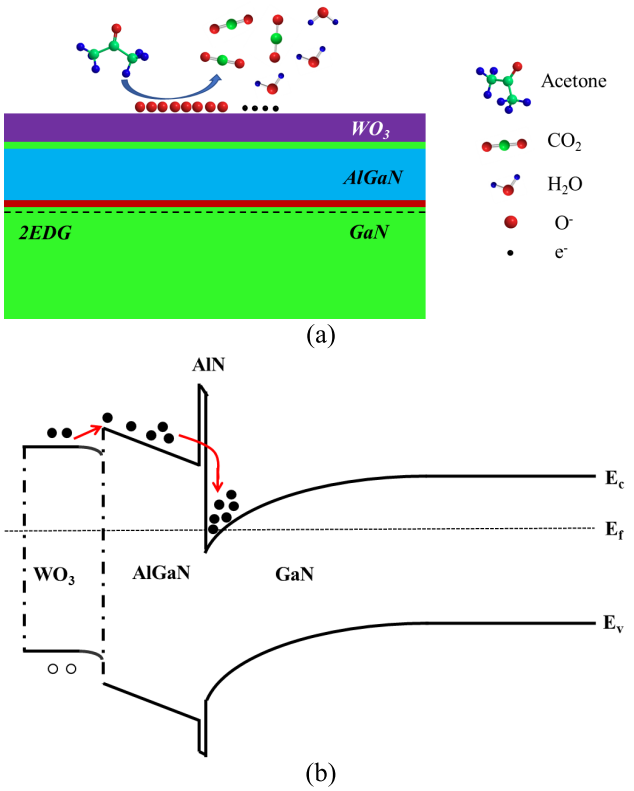

Fig. 13. (a) Schematic of oxidation of acetone in the gate region of the WO_3/AlGaN/GaN sensor. (b) Energy band diagram of WO_3/AlGaN/GaN heterostructure. E_C: conduction band edge, E_V: valance band edge, and E_f: Fermi level.

(e.g., Pt, Pd, or Ag), dissociate and release electrons [30], [39], [40]. When the sensor is in contact with air as shown in Fig. 13, because of the presence of oxygen in the air, oxygen adsorption on the WO_3 surface traps electron from the conduction band of the semiconductor to form oxygen species (O_2^-, O^-, or O^{2-}) [35], [40]. In this ionosorption process, this doubly charged adsorbed oxygen O^{2-} is not stable when the doubly charged oxygen ions do not react immediately or are trapped by oxygen vacancies

$$O_2(\text{gas}) \leftrightharpoons O_2(\text{ads}) \quad (1)$$

$$O_2(\text{ads}) + e^- \rightleftharpoons O_2^-(\text{ads}) \quad (2)$$

$$O_2^-(\text{ads}) + e^- \rightleftharpoons 2O^-(\text{ads}) \quad (3)$$

$$O^-(\text{ads}) + e^- \rightleftharpoons O^{2-}(\text{ads}). \quad (4)$$

Such oxygen ions will act as electron trap on the sensing surface. When the temperature of the sensing area is above 150 °C, O^- dominates during the ionosorption process. The reaction rate of O^- is greater than O^{2-}. Accordingly, once the sensor is exposed to acetone gas, the acetone molecules react with the adsorbed oxygen ions O^-, then produce CO_2 and H_2O, and release electrons following (5) [10], [41], [42]. Releasing electrons in the conduction band leads to the bending of the band toward lower energy and move to 2-DEG channel, which increases the drain current after exposure to acetone gas

$$CH_3COCH_3(\text{gas}) + 8O^- \rightarrow 3CO_2 + 3H_2O + 8e^-. \quad (5)$$

In addition, the surface states would be altered by the polar acetone molecules, which would manipulate the 2-DEG concentration. Therefore, the surface potential of the WO_3 and AlGaN are changed, resulting in the variation in the drain current of the HEMT device. The changed surface potential can mathematically be represented by the Helmholtz model

$$\Delta V = \frac{N_S\, p(\cos\theta)}{\varepsilon\varepsilon_0} \quad (6)$$

where p is the dipole moment, N_S is the dipole density per unit area, θ is the angle between the dipole and the normal surface, ε is the relative permittivity of the material, and ε_0 is the permittivity of free space. The surface potential is majorly affected by the value of p/ε of the polar molecules. Compared with other gases such as ethanol and ammonia, acetone is one of the most polar molecules. Consequently, the sensitivity of the device to acetone is larger than for other gases.

IV. Conclusion

The suspended AlGaN/GaN HEMT sensors with a tungsten trioxide (WO_3) nanofilm modified gate were developed for ppm-level acetone gas detection. The temperature of the sensor can be adjusted by the integrated microheater, and the membrane structure was designed for operation at high temperature and low power. At 300 °C, a drain current change ΔI_{DS} of 0.31 mA and a high sensitivity of 25.7% for 1000-ppm acetone were observed. Transient measurements indicated stable operation and good repeatability at different temperatures. For 1000-ppm acetone concentration, t_{Res} (t_{Rec}) reduced from 147 (656) s at $V_H = 3.5$ V (210 °C) to 48 (319) s at $V_H = 4$ V (300 °C). Moreover, the response to 1000-ppm acetone gas was significantly larger than for ethanol, ammonia, and CO gases at the same 1000-ppm concentration. These performances reveal that GaN-based HEMT sensors are a promising approach for gas sensing in industrial and medical applications.

Acknowledgment

The authors would like to thank Prof. J. Wang and the staff of the Institute of Semiconductors, Chinese Academy of Sciences, Beijing, China, for their assistance in device fabrication and X. Guo from the Institute of Microelectronics, Chinese Academy of Sciences, for the packaging.

REFERENCES

[1] X. Liu, J. Hu, B. Cheng, H. Qin, and M. Jiang, "Acetone gas sensing properties of $SmFe_{1-x}Mg_xO_3$ perovskite oxides," *Sens. Actuators B, Chem.*, vol. 134, no. 2, pp. 483–487, Sep. 2008.

[2] T. E. Kiehn, E. M. Bernard, J. Gold, and D. Armstrong, "Candidiasis: Detection by gas-liquid chromatography of D-arabinitol, a fungal metabolite, in human serum," *Sci.*, vol. 206, no. 4418, pp. 577–580, Nov. 1979.

[3] S. M. Hicks and A. J. Killard, "Electrochemical impedance characterisation of tungsten trioxide–polyaniline nanocomposites for room temperature acetone sensing," *Sens. Actuators B, Chem.*, vol. 194, pp. 283–289, Apr. 2014.

[4] L. Ciaffoni *et al.*, "Demonstration of a mid-infrared cavity enhanced absorption spectrometer for breath acetone detection," *Anal. Chem.*, vol. 85, no. 2, pp. 846–850, Dec. 2012.

[5] S. B. Khan, M. Faisal, M. M. Rahman, and A. Jamal, "Low-temperature growth of ZnO nanoparticles: Photocatalyst and acetone sensor," *Talanta*, vol. 85, no. 2, pp. 943–949, Aug. 2011.

[6] P. P. Sahay, "Zinc oxide thin film gas sensor for detection of acetone," *J. Mater. Sci.*, vol. 40, no. 16, pp. 4383–4385, Aug. 2005.

[7] Y. Zeng *et al.*, "Growth and selective acetone detection based on ZnO nanorod arrays," *Sens. Actuators B, Chem.*, vol. 143, no. 1, pp. 93–98, Dec. 2009.

[8] L. Qin *et al.*, "The template-free synthesis of square-shaped SnO_2 nanowires: The temperature effect and acetone gas sensors," *Nanotechnology*, vol. 19, no. 18, Apr. 2008, Art. no. 185705.

[9] S. F. Bamsaoud, S. B. Rane, R. N. Karekar, and R. C. Aiyer, "Nano particulate SnO_2 based resistive films as a hydrogen and acetone vapour sensor," *Sens. Actuators B, Chem.*, vol. 153, no. 2, pp. 382–391, Apr. 2011.

[10] S.-J. Choi, B.-H. Jang, S.-J. Lee, B. K. Min, A. Rothschild, and I.-D. Kim, "Selective detection of acetone and hydrogen sulfide for the diagnosis of diabetes and halitosis using SnO_2 nanofibers functionalized with reduced graphene oxide nanosheets," *ACS Appl. Mater. Inter.*, vol. 6, no. 4, pp. 2588–2597, Jan. 2014.

[11] M. Righettoni, A. Tricoli, and S. E. Pratsinis, "Si: WO_3 sensors for highly selective detection of acetone for easy diagnosis of diabetes by breath analysis," *Anal. Chem.*, vol. 82, no. 9, pp. 3581–3587, Apr. 2010.

[12] L. Wang, A. Teleki, S. E. Pratsinis, and P. I. Gouma, "Ferroelectric WO_3 nanoparticles for acetone selective detection," *Chem. Mater.*, vol. 20, no. 15, pp. 4794–4796, Jul. 2008.

[13] S.-J. Choi *et al.*, "Selective diagnosis of diabetes using Pt-functionalized WO_3 hemitube networks as a sensing layer of acetone in exhaled breath," *Anal. Chem.*, vol. 85, no. 3, pp. 1792–1796, Dec. 2013.

[14] C. Wang *et al.*, "Ultrasensitive and low detection limit of acetone gas sensor based on W-doped NiO hierarchical nanostructure," *Sens. Actuators B, Chem.*, vol. 220, pp. 59–67, Dec. 2015.

[15] Y. Lu *et al.*, "Synthesis of cactus-like NiO nanostructure and their gas-sensing properties," *Mater. Lett.*, vol. 164, pp. 48–51, Feb. 2016.

[16] L. Wang, T. Fei, Z. Lou, and T. Zhang, "Three-dimensional hierarchical flowerlike a-Fe_2O_3 nanostructures: Synthesis and ethanol-sensing properties," *ACS Appl. Mater. Inter.*, vol. 3, no. 12, pp. 4689–4694, Nov. 2011.

[17] C. Zhu, Y. Chen, R. Wang, L. Wang, M. Cao, and X. Shi, "Synthesis and enhanced ethanol sensing properties of α-Fe_2O_3/ZnO heteronanostructures," *Sens. Actuators B, Chem.*, vol. 140, no. 1, pp. 185–189, Jun. 2009.

[18] L. Wang, Z. Lou, J. Deng, R. Zhang, and T. Zhang, "Ethanol gas detection using a yolk-shell (Core-Shell) a-Fe_2O_3 nanospheres as sensing material," *ACS Appl. Mater. Inter.*, vol. 7, no. 23, pp. 13098–13104, May 2015.

[19] A. Mirzaei, K. Janghorban, B. Hashemi, M. Bonyani, S. Leonardi, and G. Neri, "Highly stable and selective ethanol sensor based on α-Fe_2O_3 nanoparticles prepared by Pechini sol–gel method," *Ceramics Int.*, vol. 42, no. 5, pp. 6136–6144, Apr. 2016.

[20] G. Eranna, *Metal Oxide Nanostructures as Gas Sensing Devices*. Boca Raton, FL, USA: CRC Press, 2016.

[21] B. S. Kang *et al.*, "Hydrogen-induced reversible changes in drain current in Sc_2O_3/AlGaN/GaN high electron mobility transistors," *Appl. Phys. Lett.*, vol. 84, no. 23, pp. 4635–4637, May 2004.

[22] S. C. Hung, C. W. Chen, C. Y. Shieh, G. C. Chi, R. Fan, and S. J. Pearton, "High sensitivity carbon monoxide sensors made by zinc oxide modified gated GaN/AlGaN high electron mobility transistors under room temperature," *Appl. Phys. Lett.*, vol. 98, no. 22, Jun. 2011, Art. no. 223504.

[23] C.-F. Lo *et al.*, "Carbon monoxide detection sensitivity of ZnO nanorod-gated AlGaN/GaN high electron mobility transistors in different temperature environments," *J. Vacuum Sci. Technol. B*, vol. 30, no. 1, Dec. 2012, Art. no. 010606.

[24] S. C. Hung, W. Y. Woon, S. M. Lan, F. Ren, and S. J. Pearton, "Characteristics of carbon monoxide sensors made by polar and nonpolar zinc oxide nanowires gated AlGaN/GaN high electron mobility transistor," *Appl. Phys. Lett.*, vol. 103, no. 8, Aug. 2013, Art. no. 083506.

[25] Y. Halfaya *et al.*, "Investigation of the performance of HEMT-based NO, NO_2 and NH_3 exhaust gas sensors for automotive antipollution systems," *Sensors*, vol. 16, no. 3, p. 273, Feb. 2016.

[26] C. Bishop *et al.*, "Experimental study and device design of NO, NO_2, and NH_3 gas detection for a wide dynamic and large temperature range using Pt/AlGaN/GaN HEMT," *IEEE Sensors J.*, vol. 16, no. 18, pp. 6828–6838, Sep. 2016.

[27] P. Offermans and R. Vitushinsky, "NO_2 detection with AlGaN/GaN 2DEG channels for air quality monitoring," *IEEE Sensors J.*, vol. 13, no. 8, pp. 2823–2827, Aug. 2013.

[28] P. Offermans, R. Vitushinsky, M. Crego-Calama, and S. H. Brongersma, "Ultra-sensitive NO_2 detection with AlGaN/GaN 2DEG channels for air quality monitoring," in *Proc. IEEE Sensors*, Oct. 2012, pp. 905–907.

[29] P.-C. Chou *et al.*, "Study of an electroless plating (EP)-based Pt/AlGaN/GaN Schottky diode-type ammonia sensor," *Sens. Actuators B, Chem.*, vol. 203, pp. 258–262, Nov. 2014.

[30] T.-Y. Chen *et al.*, "On an ammonia gas sensor based on a Pt/AlGaN heterostructure field-effect transistor," *IEEE Electron Device Lett.*, vol. 33, no. 4, pp. 612–614, Apr. 2012. doi: 10.1109/LED.2012.2184832.

[31] Y. Y. Xi *et al.*, "Methane detection using Pt-gated AlGaN/GaN high electron mobility transistor based Schottky diodes," *J. Vacuum Sci. Technol. B*, vol. 31, no. 3, May 2013, Art. no. 032203.

[32] R. Sokolovskij *et al.*, "Hydrogen sulfide detection properties of Pt-gated AlGaN/GaN HEMT-sensor," *Sens. Actuators B, Chem.*, vol. 274, pp. 636–644, Nov. 2018.

[33] R. Sokolovskij *et al.*, "Pt-AlGaN/GaN HEMT-sensor for hydrogen sulfide (H_2S) detection," *Proceedings*, vol. 1, no. 4, p. 463, Aug. 2017.

[34] J. Schalwig, G. Müller, M. Eickhoff, O. Ambacher, and M. Stutzmann "Gas sensitive GaN/AlGaN-heterostructures," *Sens. Actuators B, Chem.*, vol. 87, no. 3, pp. 425–430, 2002.

[35] S. Das, S. Ghosh, R. Kumar, A. Bag, and D. Biswas, "Highly sensitive acetone sensor based on Pd/AlGaN/GaN resistive device grown by plasma-assisted molecular beam epitaxy," *IEEE Trans. Electron Devices*, vol. 64, no. 11, pp. 4650–4656, Nov. 2017.

[36] P. Offermans *et al.*, "Suspended AlGaN/GaN membrane devices with recessed open gate areas for ultra-low-power air quality monitoring," in *IEDM Tech. Dig.*, Dec. 2015, pp. 33.6.1–33.6.4.

[37] C. Silvestri, P. Picciafoco, B. Morana, F. Santagata, G. Q. Zhang, and P. M. Sarro, "Electro-thermal simulation and characterization of vertically aligned CNTs directly grown on a suspended microhoplate for thermal management applications," in *Proc. IEEE Sensors*, Nov. 2014, pp. 827–830.

[38] S. Das, A. Bag, R. Kumar, and D. Biswas, "Fast response (7.6s) acetone sensing by InGaN/GaN on Si (111) at 373 K," *IEEE Electron Device Lett.*, vol. 38, no. 3, pp. 383–386, Mar. 2017.

[39] J. Schalwig, G. Müller, M. Eickhoff, O. Ambacher, and M. Stutzmann, "Gas sensitive GaN/AlGaN-heterostructures," *Sens. Actuators B, Chem.*, vol. 87, no. 3, pp. 425–430, Dec. 2002.

[40] B. Urasinska-Wojcik, T. A. Vincent, M. F. Chowdhury, and J. W. Gardner, "Ultrasensitive WO_3 gas sensors for NO_2 detection in air and low oxygen environment," *Sens. Actuators B, Chem.*, vol. 239, pp. 1051–1059, Feb. 2017.

[41] Z. Zhang, L. Zhu, Z. Wen, and Z. Ye, "Controllable synthesis of Co_3O_4 crossed nanosheet arrays toward an acetone gas sensor," *Sens. Actuators B, Chem.*, vol. 238, pp. 1052–1059, Jan. 2017.

[42] B. Bhowmik, H.-J. Fecht, and P. Bhattacharyya, "Vertical mode gas sensing performance of TiO_2 nanotube array by tuning of surface area and carrier transport length," *IEEE Sensors J.*, vol. 15, no. 10, pp. 5919–5926, Oct. 2015.